Journal of Applied Sciences

ISSN 1812-5654

science alert

ANSInet
an open access publisher
http://ansinet.com

Journal of Applied Sciences 9 (9): 1658-1667, 2009
ISSN 1812-5654
© 2009 Asian Network for Scientific Information

Analysis of Capacitive Microelectromechanical System Accelerometer Proposed with Voltage Reference in Read-Out Circuit

M.A. Miskam, O. Sidek and A.Z. Ruhaifi
Engineering Campus, Collaborative Microelectronic Design Excellence Centre,
Universiti Sains Malaysia, 14300 Nibong Tebal, Sri Ampangan, Pulau Pinang, Malaysia

Abstract: This study, present the analysis of the capacitive in-plane linear comb drive microelectromechanical system (MEMS) accelerometer using system-level simulation techniques, Finite Element Method (FEM) and simple analytical modeling. The silicon on insulator high aspect ratio micromachining (SOI-HARM) process is use to fabricate the device. The behavior of the device will be simulated using DC operating point analysis, mechanical resonance frequency analysis, vary analysis, DC transfer analysis and transient analysis. The results agree well with the results obtained by Architect, FEM and analytical analysis. The design methodology and circuit implementation of bandgap reference for MEMS accelerometer also will be described. A low variation in voltage reference is proposed and simulated using Silterra 0.13 μm CMOS technology. The voltage reference is operated with a supply voltage of 2.5 V to achieve an output reference of 1.17949 V. The circuit has achieved a very small variation in reference voltage of about ±0.36 mV resulting from temperature changes between -50 to 100°C and maximum PSSR of -49.03 dB.

Key words: MEMS, microaccelerometer, inertial sensors, micromachined sensors, silicon sensors

INTRODUCTION

A micro-electromechanical system (MEMS) is a process technology used to create tiny integrated devices or systems that combine mechanical and electrical components. They are fabricated using Integrated Circuit (IC) batch processing techniques and can range in size from micrometers to millimeters. These devices (or systems) have the ability to sense, control and actuate on the micro scale and generate effects on the macro scale. MEMS technology exhibits many advantages indigenous to IC technology such as cost, size and weight reduction (Fokhrul *et al*., 2008). MEMS has been identified as one of the most promising technologies for the 21st century and has the potential to revolutionize both industrial and consumer products by combining silicon-based microelectronics with micromachining technology (Bernhard and Howe, 1996).

Accelerometers are probably the most common application of MEMS technology, as they only require sensing the movement of a mass subject to acceleration (Dan Haronian, 2000). Accelerometers which can be classified according to their transduction mechanisms have been used in microaccelerometers i.e., piezoresistive, tunneling, resonant, thermal, optical, electromagnetic, piezoelectric and capacitive. Accelerometers that implement capacitive sensing output measure acceleration based on a change in capacitance due to a moving plate or sensing element. These devices are used across a very wide range of applications i.e., automobile air bags (Zimmermann *et al*., 1995), navigation (Josselin *et al*., 1999) and instrumentation (Tan and Park, 2002). This method of sensing is able to sense with high accuracy and stability.

In the past several years, extensive research has been done on the design, fabrication, modeling and structural analysis to increase the sensitivity of the device. For example, the sensitivity of the capacitive accelerometer can be improved by increasing the proof mass and the number of sensing fingers arrays and decreasing the spring stiffness. Majority of the effort goes towards improving the performance characteristics and reducing manufacturing cost (Bernhard and Howe, 1996; Gang *et al*., 1999; Junseok *et al*., 2005; Vivek *et al*., 2006; Seiji *et al*., 2007; Chih-Ming *et al*., 2008; Krishnamoorthy *et al*., 2008; John *et al*., 2008).

Voltage reference is an important building block for MEMS accelerometer read-out circuit architecture (Fig. 1) because a stable bias voltage or power supply source is needed. A reference circuit is an independent voltage or

Corresponding Author: Muhamad Azman Miskam, Engineering Campus, Collaborative Microelectronic Design Excellence Centre, Universiti Sains Malaysia, 14300 Nibong Tebal, Sri Ampangan, Pulau Pinang, Malaysia
Tel: +604-5995819 Fax: +604-5930920

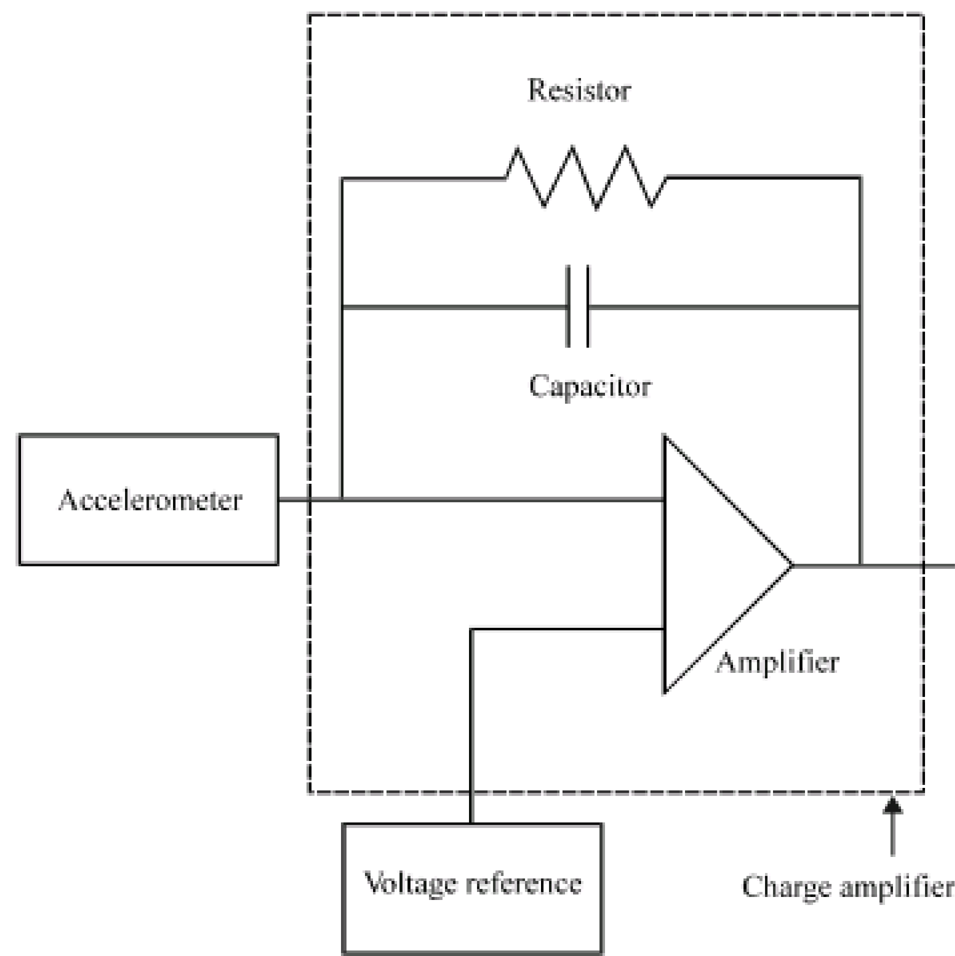

Fig. 1: Read-out circuit architecture for MEMS accelerometer

current source that has a high degree of precision and stability. A conventional bandgap reference adds the forward-bias voltage across p-n diode and that voltage is weighted by adjusting the ratio of two resistors. The output of the reference voltage will be unstable in case of improper weighing. Thus, the bandgap reference should utilize the negative-temperature-coefficient unsilicided N-island resistor and unsilicided P-island resistor as a weighed component. This resistor ratio can effectively eliminate the temperature drift of the reference voltage (Rasoul and Atarodi, 2003).

The aim of this study is to analyze the capacitive MEMS accelerometer using system-level simulation techniques, FEM and simple analytical modeling. This simulation study will explain the behavior of the designed MEMS accelerometer using DC operating point analysis, mechanical resonance frequency analysis, vary analysis, DC transfer analysis and transient analysis. Simulation results are discussed and performance of the design is presented. The design methodology and circuit implementation of bandgap reference for MEMS accelerometer also will be described because this voltage reference is an important building block in read-out circuit for the designed MEMS accelerometer.

MATERIALS AND METHODS

Proposed structure: The sensor transfers the position change into capacitive variation to detect acceleration. It is composed of a proof mass suspended by four straight beams and comb fingers (Fig. 2). The central part of this mass is perforated to improve the technological release step and the air damping. The total device structure size is 1021 by 1295 μm. The accelerometer has a proof mass of 140 by 1295 μm with multiple 10 by 10 μm releasing holes. The 100 movable sensing fingers and fixed fingers are the same size of 350 μm long and 6 μm wide. Each straight beam is 246 μm long and 2 μm wide. The completely released structure is uniformly 60 μm thick. The silicon used as mechanical structures has a property elastic modulus of 1.70×10^5 MPa, Poison's ratio of 2.70×10^{-1} and density of 2.34×10^{-15} kg μm^{-3}.

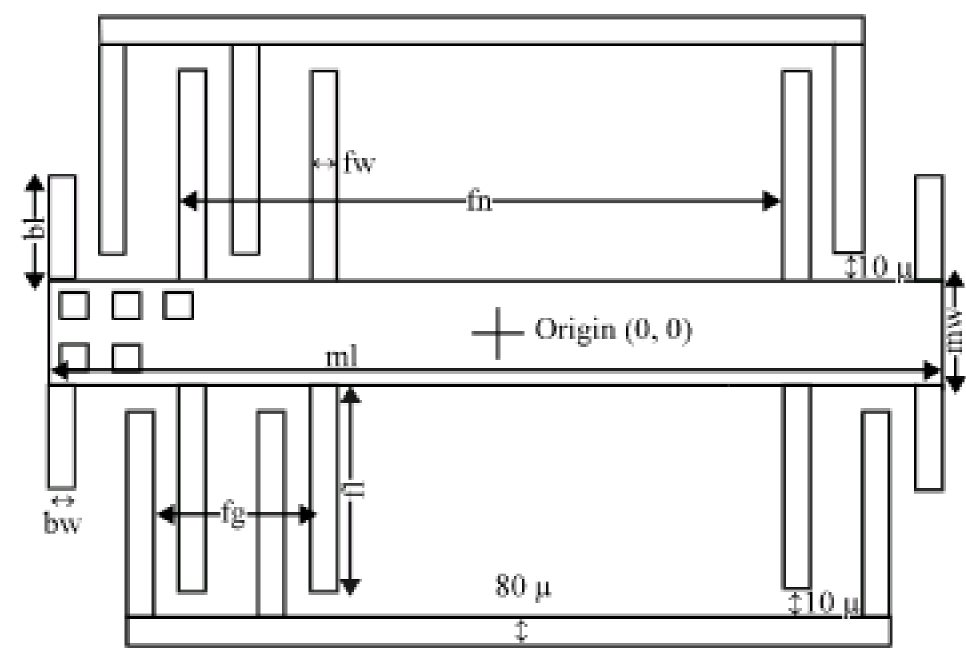

Fig. 2: Schematic diagram of comb drive MEMS accelerometer designed structure

Modeling and simulation: Capacitive comb drive accelerometer has been designed, modeled and simulated using Architect and Analyzer modules in commercial software, CoventorWare®2006. Architect is a system-level design environment that benefits from the combination of MEMS behavioral models and the IC circuit components. Analyzer is a solver solution for physics simulation starts with a 3-D model created from a 2-D layout and process file, or a model imported from a third-party solid modeling tool. The initial process starts with schematic creation using Architect module (Fig. 3).

The silicon on insulator high aspect ratio micromachining (SOI-HARM) process is used to fabricate the device. This process is a metal-last process based on the deep dry etching (or DRIE) of silicon. A process editor is used to create 3-D model building by defining various parameters such as substrate, deposition of selected material, etching-type, depth and masks. The completed schematic is transformed into a 2-D layout and 3-D solid model. This solid model is then meshed for further finite element analysis (Fig. 4).

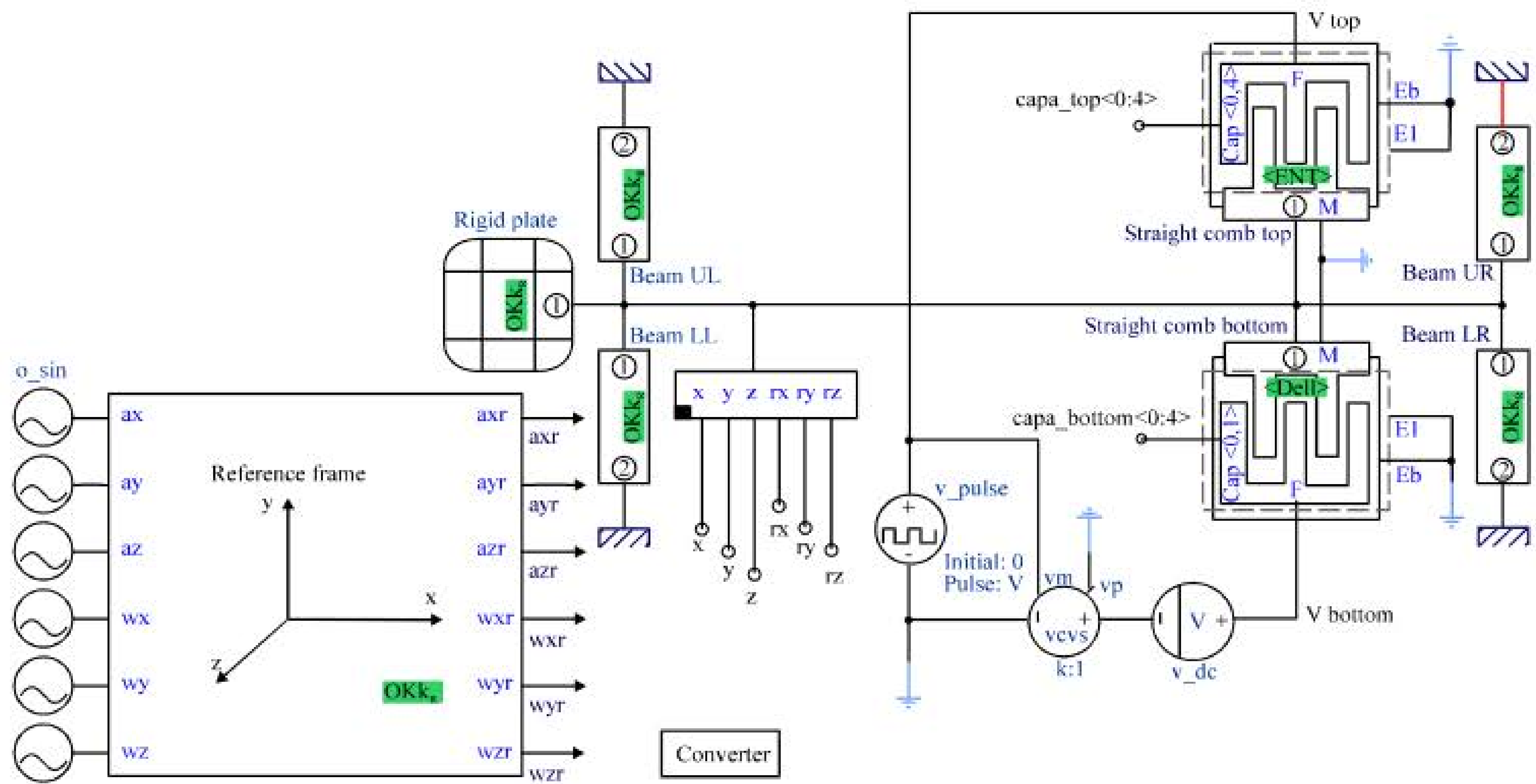

Fig. 3: Schematic drawing of capacitive comb drives MEMS accelerometer in Architect Module

Fig. 4: Meshed model of capacitive comb drive MEMS accelerometer

The behavior of the device will be simulated using DC operating point analysis, mechanical resonance frequency analysis, vary analysis, DC transfer analysis and transient analysis.

DC operating point analysis: DC operating point analysis is run to find values of the system during steady state at time zero. The DC bias values of the electrical component and the initial displacements of the mechanical components are determined from this analysis. The analysis is repeated for several times by using various voltages. The electrostatic force can be calculated by:

$$F_{elec} = \frac{1}{4}\eta\varepsilon_o\varepsilon_r h(y_o + y)\left(\frac{1}{(x_+ - x)^2} - \frac{1}{(x_- + x)^2}\right)V^2 \quad (1)$$

The restoring elastic force can be calculated by:

$$F_{elas} = k_{mech}x = 4Eh\frac{w_b^3}{L_b^3}x \quad (2)$$

At equilibrium, the total force acting on the movable structure in x-axis is zero:

$$\frac{1}{4}\eta\varepsilon_o\varepsilon_r h(y_o + y)\left(\frac{1}{(x_+ - x)^2} - \frac{1}{(x_- + x)^2}\right)V^2 - 4Eh\frac{w_b^3}{L_b^3}x = 0 \quad (3)$$

By using Eq. 3, the accelerometer displacement in x direction for a certain voltage can be calculated. The effective electrostatic spring constant is as follows (Ka Nang *et al*., 2003):

$$k_{elec} = -\frac{1}{2}\eta\varepsilon_o\varepsilon_r h(y_o + y)\left(\frac{1}{(x_+ - x)^3} - \frac{1}{(x_- + x)^3}\right)V^2 \quad (4)$$

The electrostatic force is in the opposite direction of the mechanical spring force, so the actual effective spring constant is as follows:

$$k_{eff} = k_{mech} + k_{elec} \quad (5)$$

$$k_{eff} = 4Eh\frac{w_b^3}{L_b^3} - \frac{1}{2}\eta\varepsilon_o\varepsilon_r h(y_o + y)\left(\frac{1}{(x_+ - x)^3} - \frac{1}{(x_- + x)^3}\right)V^2 \quad (6)$$

Instability occurs when the actual effective spring constant is less than zero. The voltage causes the instability to occur is as follows:

$$V_{critical} = \sqrt{\frac{k_{mech}}{D}} \quad (7)$$

$$D = \frac{1}{2}\eta\varepsilon_o\varepsilon_r h(y_o + y)\left(\frac{1}{(x_+ - x)^3} - \frac{1}{(x_- + x)^3}\right) \quad (8)$$

Mechanical resonance frequency analysis: This analysis is run to obtain resonant frequency of the MEMS accelerometer. The analysis starts with DC operating point analysis running with all voltage sources set to zero and followed by frequency analysis with mechanical excitation. This analysis linearizes the models around the values that can be found from DC analysis and sweeps a frequency range to determine the frequency response. This analysis is repeated for several times by applying various DC voltages to the straight comb bottom to see the influence of DC voltage on the resonant frequency of the accelerometer. Without DC voltage applied, the resonant frequency f_r of the accelerometer is given by the following equation:

$$f_r = \frac{1}{2\pi}\sqrt{\frac{k_{eff}}{m_s}} \quad (9)$$

where, by m_s is as follows:

$$m_s = \rho h\left[W_m L_m + \eta W_f L_f + 4W_b L_b - (L_m - \eta_x H)x(W_m - \eta_y H)\right] \quad (10)$$

Vary analysis: In this analysis, the width and length of the beams are varied and the impact on the x resonance frequency is investigated. Theoretically, the resonance frequency should increase as the width increases and the length decreases. The resonant frequency f_r of the accelerometer can be calculated by using Eq. 7 and 8.

DC transfer analysis: A DC transfer analysis is conducted by sweeping an independent source over a sweep range. During this analysis, all voltage sources are set to zero and acceleration is applied relative to x-axis of the reference frame to see its influence on the MEMS accelerometer. The displacement sensitivity S_d of the accelerometer, which is defined as the displacement of movable fingers per unit gravity acceleration, g along the sensitive direction, can be obtained by the following equation (Xingguo *et al*., 2005):

$$S_d = \frac{m_s g}{k_{mech}} = \frac{\rho g\left[W_m L_m + \eta W_f L_f + 4W_b L_b - (L_m - \eta_x H)x(W_m - \eta_y H)L_B^3\right]}{4EW_B^3} \quad (11)$$

Dimension analysis: The performance of the accelerometer depends on the dimensions of the structure. Thus, in this analysis, the number of moveable fingers for each comb has been changed to characterize its performance. The displacement of accelerometer with different voltage applied can be used as an indicator of performance. Equation 2 is used to find the displacement, while Eq. 4 and 5 were used to calculate the voltage instability occurs.

Transient analysis: In this analysis, acceleration is applied on the structure and its response in time is observed. A basic sensing electronic circuit, consists of resistor, capacitor, diode ground and Op Amp, is added to the comb drive accelerometer to produce a usable output signal. Single-ended half-bridge capacitive sense interface

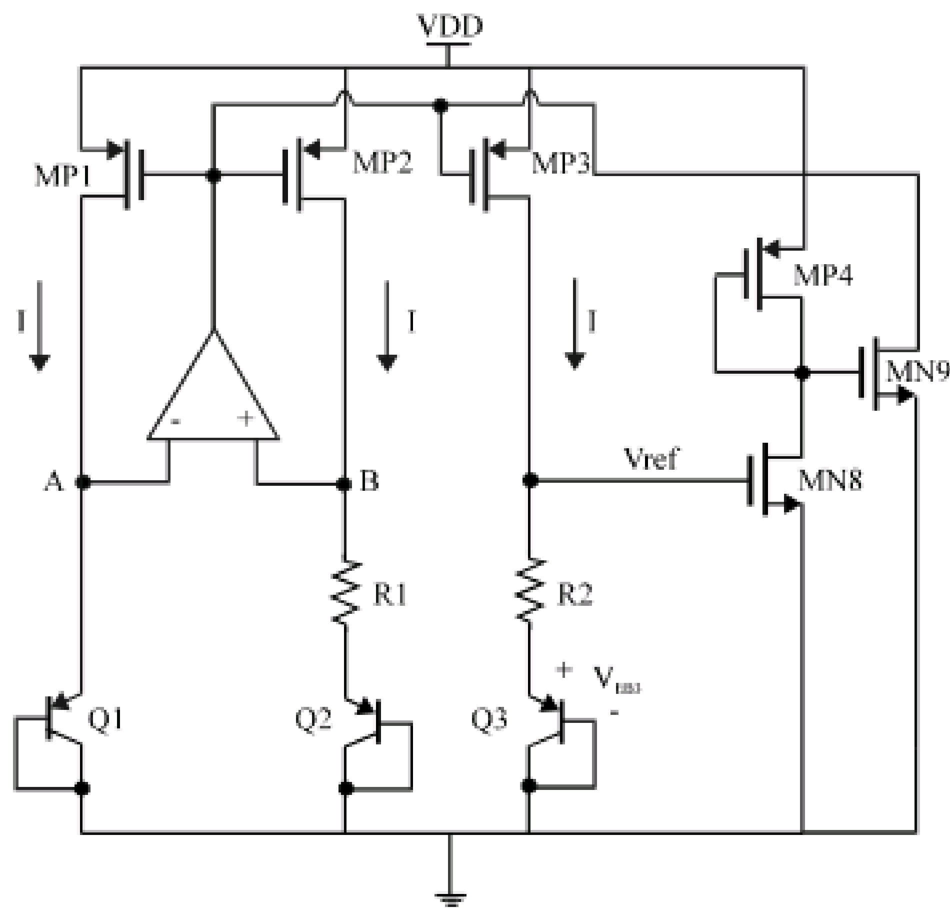

Fig. 5: Schematic diagram of bandgap reference circuit

is commonly used to translate the displacement into output voltage. The sensitivity of accelerometer, which is defined as the ratio of output voltage over the input acceleration, can be obtained through the transient analysis. The analysis starts with the voltage pulse value set to 1 V. The acceleration control source that used in the DC transfer analysis is replaced by a pulse. Some damping is added to the rigid plate, as it is useful to smooth the x displacement response. This amount is near the critical damping. The probe tool is used to view displacement in x direction, acceleration and output voltage V_{demod} of the peak detector.

Proposed design for voltage reference: The circuit topology (Fig. 5) of the designed bandgap reference shows a current that is proportional to the absolute temperature is generated and added into the base emitter of Q_3. The high gain of folded cascode amplifier (Fig. 6) forces the voltages $V_A = V_B$. The voltage difference ΔV_{EB} between the emitter-base junctions of Q_1 and Q_2 is obtained using an emitter area ratio of n = 8 and equal value for currents, I. The circuit of Fig. 7 is referred to obtain ΔV_{EB} (Razavi, 2001).

$$\Delta V_{EB} = V_{EB1} - V_{EB2} = \frac{kT}{q}\ln\left[\frac{\left(\frac{I}{A}\right)}{\left(\frac{I}{nA}\right)}\right] = V_T \ln(n) \tag{12}$$

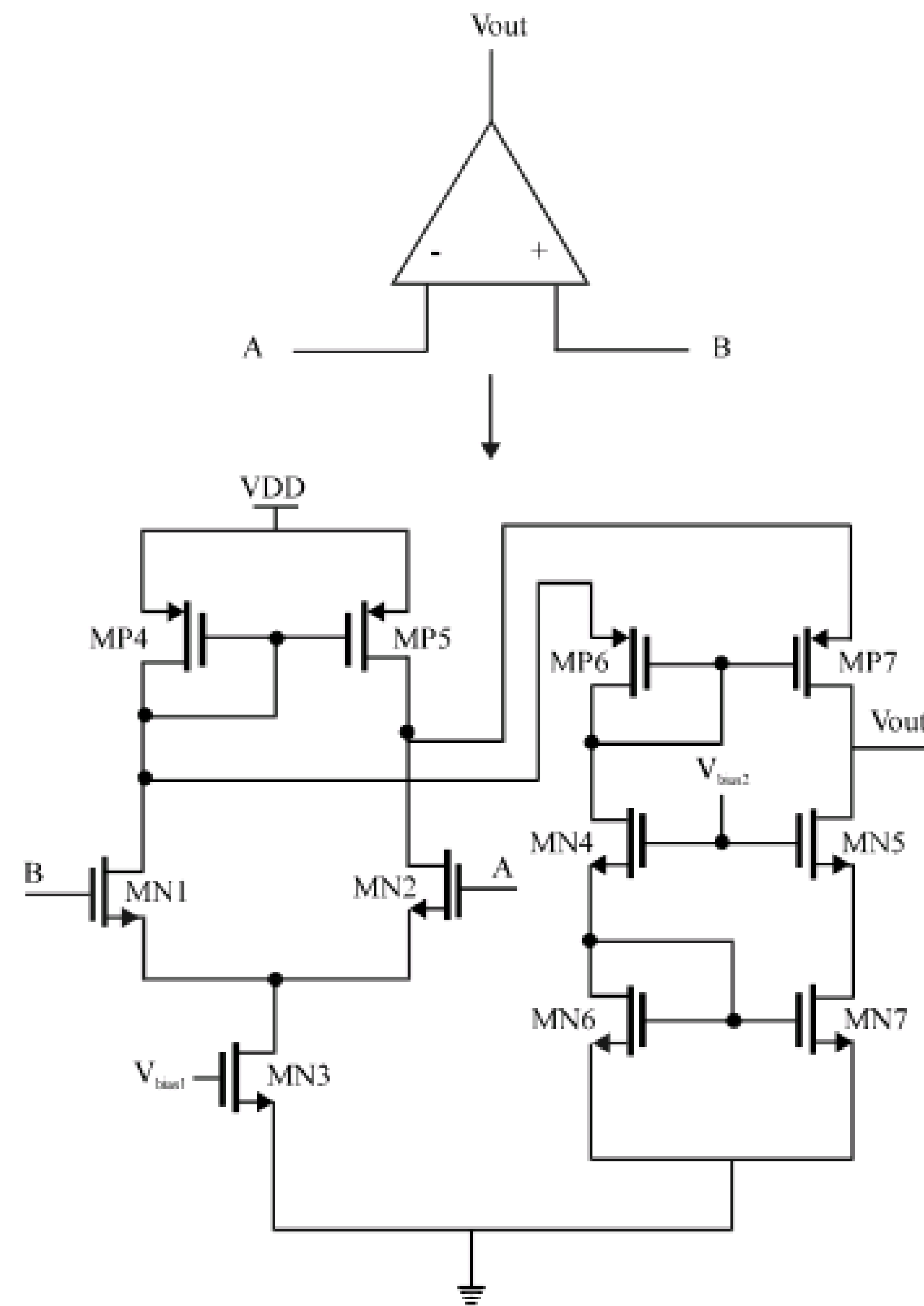

Fig. 6: Schematic diagram of folded cascode amplifier circuit

Derivation of reference voltage: Knowing that voltage at node A, V_A and voltage at node B, V_B (Fig. 5) are equal, applying Kirchhoff's Voltage Law (KVL) on node, B derives the following Eq. 13:

$$-V_B + IR_1 + V_{EB2} = 0 \tag{13}$$

The voltage appearing at node B is:

$$V_B = V_{EB1} \tag{14}$$

Then the voltage across R_1 can be expressed as:

$$IR_1 = V_A - V_{EB2} = V_{EB1} - V_{EB2} = \Delta V_{EB} \tag{15}$$

The output voltage reference can be written as follows:

$$V_{ref} = V_{EB3} + IR_2 \tag{16}$$

By substituting Eq. 15 into 16 results the reference voltage:

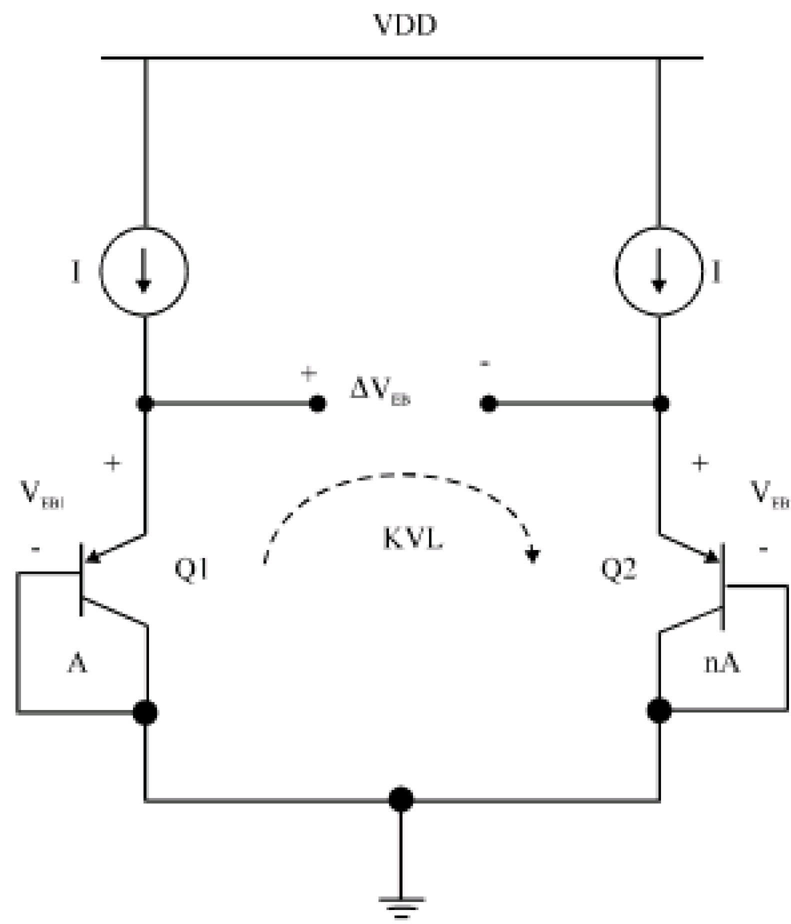

Fig. 7: Generation of proportional to absolute temperature (PTAT) voltage

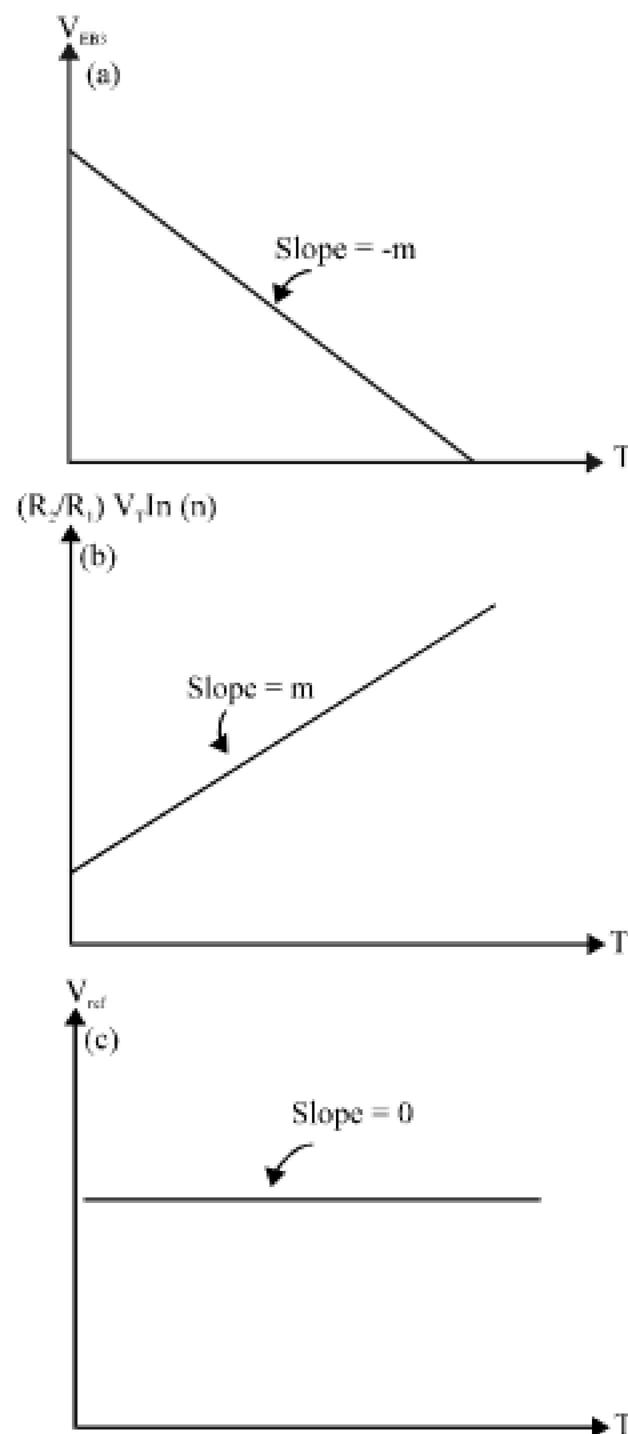

Fig. 8: (a) V_{EB3} versus temperature (T), (b) $R_1/R_2\ V_T \ln(n)$ versus temperature (T) and (c) V_{ref} versus temperature (T)

$$V_{ref} = V_{EB3} + k\Delta V_{EB} \tag{17}$$

In practice, k is the ratio of R_2/R_1 and V_{EB} is negatively PTAT while V_T has a positive temperature coefficient. The temperature coefficient can be zero by getting a proper value of k. Equation 17 can be shown in Fig. 8. The negative slope, -m of V_{EB3} (Fig. 8a) over the temperature range is obtained by simulation. It is followed by getting the exact values of R_1 and R_2 to ascertain the slope, m (Fig. 8b). The PTAT voltage increases linearly with temperature, thereby efficiently cancelling the effect of the negative linear temperature of the base emitter voltage (Rincon and Alfonso, 2001). By summing the emitter-base voltage and PTAT voltage results slope equal to zero for V_{ref} over the temperature range (Fig. 8c).

RESULTS AND DISCUSSION

DC operating point analysis: The displacement of the accelerometer increases with the increase in voltage (Fig. 9). When a DC voltage is applied to the fixed fingers, electrostatic force is generated on the proof mass. It will change the actual effective spring constant of the accelerometer from its mechanical value. The lateral electrostatic force may lead to instability if it increases more rapidly than the restoring lateral elastic force. The instability will cause the movable fingers to move laterally and collapsed to the fixed fingers. The pattern agrees with hand derived calculation and FEM. The voltage instability occurred between 2.4 and 2.45 V.

Mechanical resonance frequency analysis: The resonant frequency decreases with the increase in applied voltage (Fig. 10) due to the actual effective spring constant decreases when the voltage increases. The results notice that the deviation of the calculated resonant frequency from Architect simulation is small, which is less than 0.2%. However, the resonant frequency difference between calculation value and FEM analysis result is greater, which is in between 0.16 to 6.1%. The resonant frequency drops when the voltage rises.

Vary analysis: In this analysis, dimension of the beams is varied and the impact on the x resonance frequency is investigated. The beam width, W_b is varied from 2 to 8 µm while the beam length, L_b is varied from 246 to 396 µm. The result shows that the resonance frequency increases with the decrease in beam length and increase in beam width (Fig. 11, 12). The pattern agrees with all results from calculation, Architect analysis and FEM analysis. The deviation of the calculated resonant frequency from Architect analysis result is small, which is less than

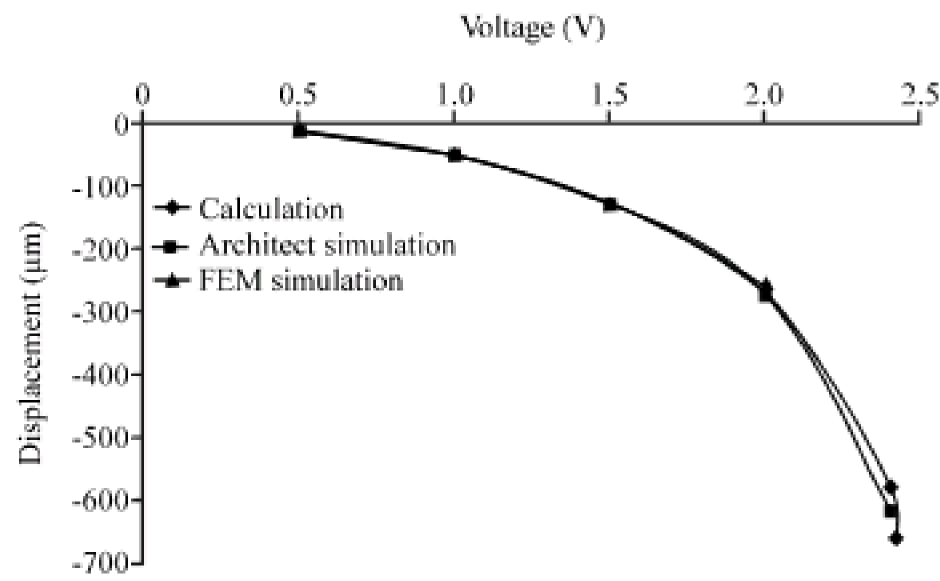

Fig. 9: DC operating point analysis of MEMS accelerometer up to 2.5 V

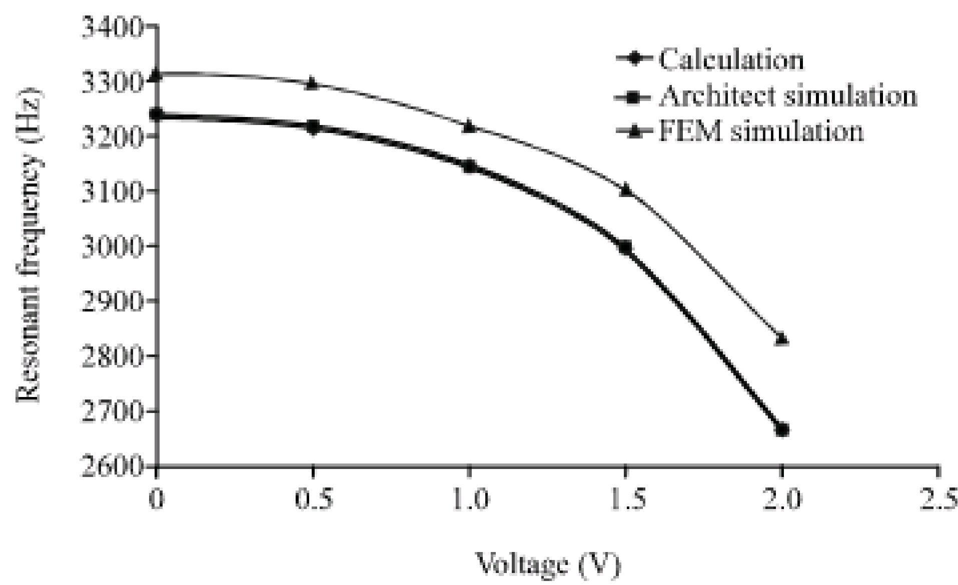

Fig. 10: Mechanical resonance frequency analysis up to 2 V

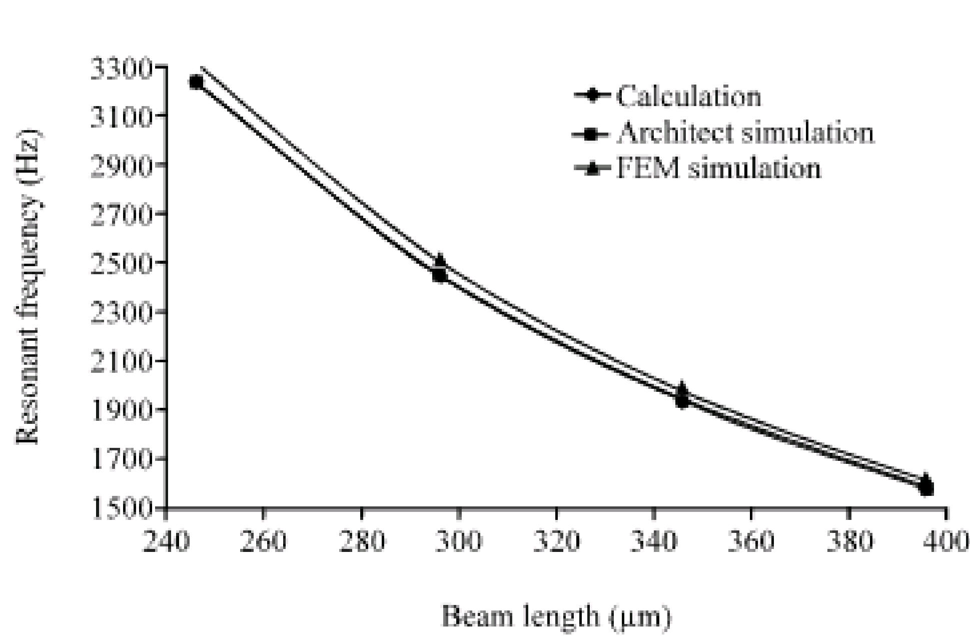

Fig. 11: Vary analysis on the beam length

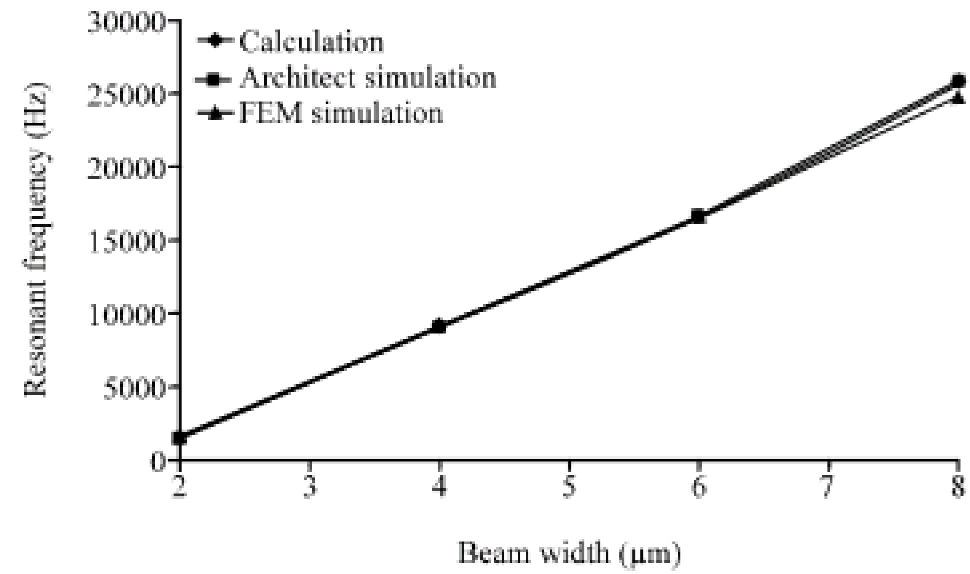

Fig. 12: Vary analysis on the beam width

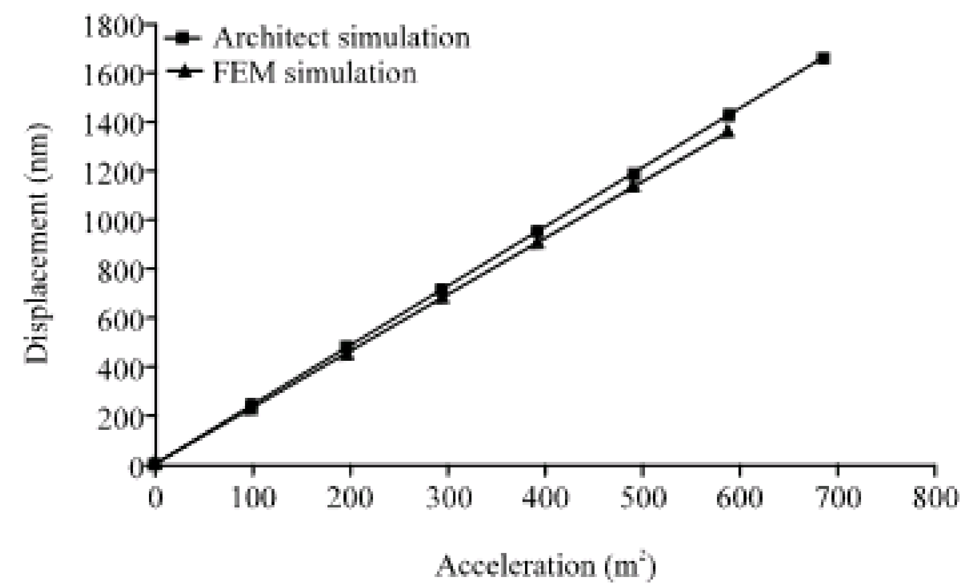

Fig. 13: Displacement of the accelerometer versus applied acceleration

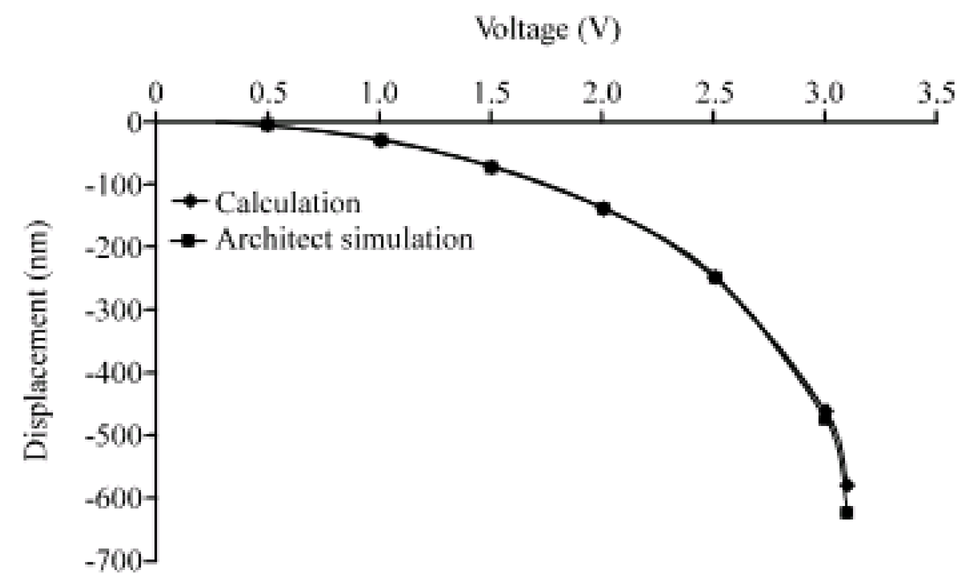

Fig. 14: Displacement of the accelerometer with respect to voltage applied

0.7%. However, the difference between calculation value and FEM analysis result is greater, which is between 0.8 and 3.4%.

DC transfer analysis: The acceleration is applied in x direction in the range of 0 to 686.7 m sec^{-2}. The result shows the displacement of the accelerometer is directly proportional to the acceleration applied (Fig. 13). The analytical result of the displacement sensitivity is 23.775 nm g^{-1}, while in simulation is 23.713 nm g^{-1}.

Dimension analysis: In this analysis, the number of movable fingers has been reduced to 60. The result shows that the displacement decreases with the increase voltage. The critical voltage where the instability occurs is between 3.1 and 3.15 V (Fig. 14). This is greater

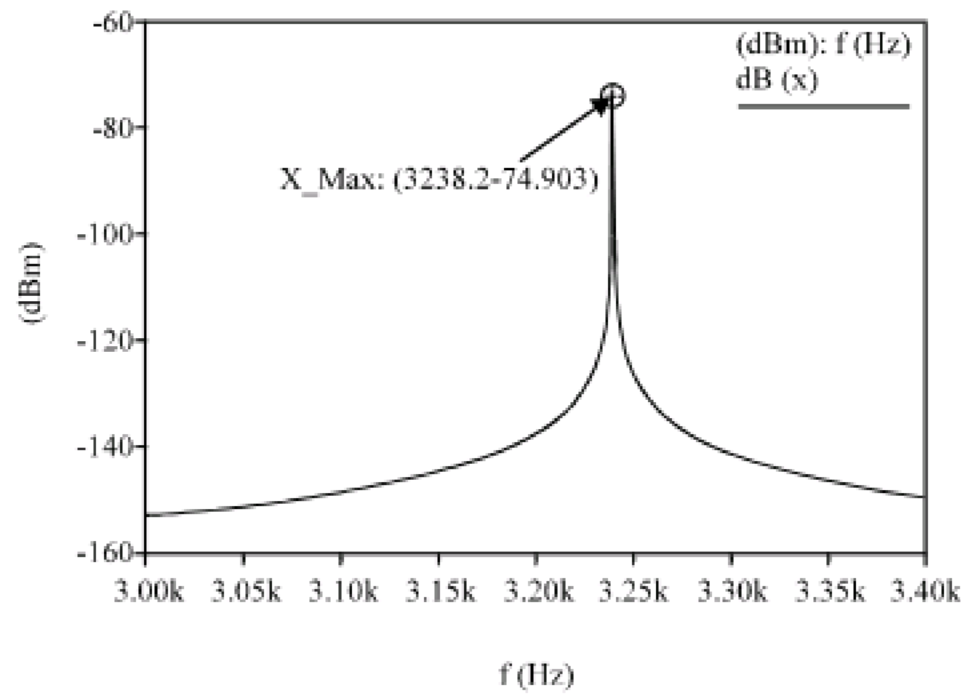

Fig. 15: Resonant frequency for 100 of movable finger

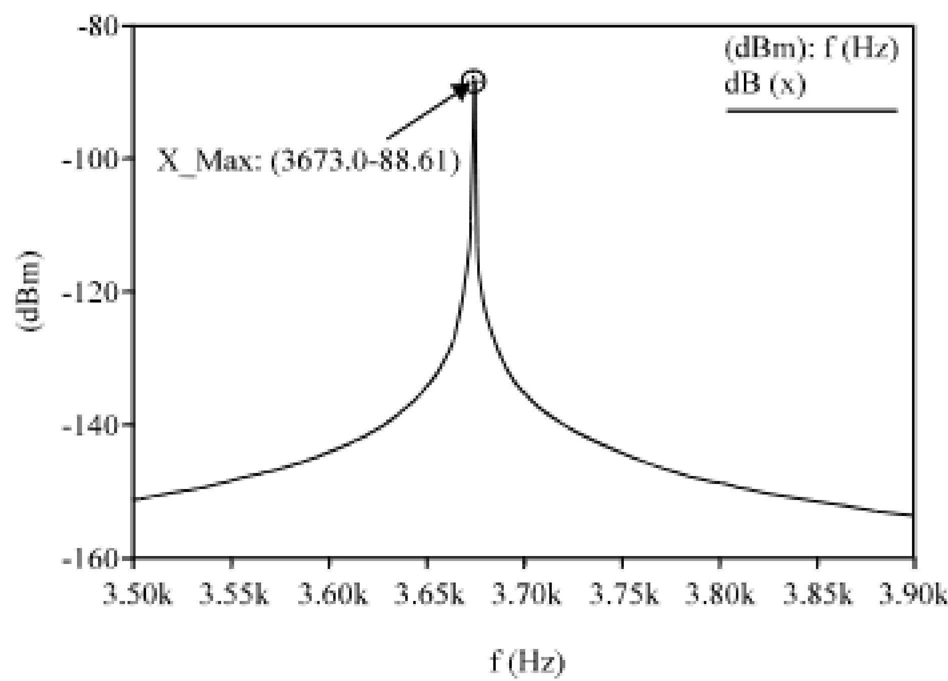

Fig. 16: Resonant frequency for 60 of movable finger

than the critical voltage of 100 movable fingers. The resonant frequency increases from 3238.2 to 3673.0 Hz (Fig. 15, 16) due to the decrease of sensing mass.

Transient analysis: The result shows that the displacement increases with the increase in acceleration (Table 1, 2). The largest acceleration that the accelerometer can detect before instabilities occur is about 48 g. The displacement and demodulated signal for this situation are 1.3487 μm and 54.535 V, respectively. The deviation of modulated signal from calculation values and Architect simulation values is at about 2.7%.

Voltage reference simulation: Various simulations were performed in a standard 0.13 μm CMOS process to analyze the effects of the process variation on the generated voltage reference in five different process corners including TT (Typical), SS (Slow-Slow), FF (Fast-Fast), FS (Fast-Slow) and SF (Slow-Fast). The reference voltage

Table 1: Transient analysis of MEMS accelerometer using calculation

Variables (calculation)	Applied acceleration = 19.62 m sec^{-2}	Applied acceleration = 470.88 m sec^{-2}
C1	5.2316 pF	3.8964 pF
C2	5.4473 pF	15.037 pF
X	-49.368 nm	-1.3487 μm
Vmod	2.1569 V_{PP}	109.7 V_{PP}

Table 2: Transient analysis of MEMS accelerometer using architect simulation

Variables (simulation)	Applied acceleration = 19.62 m sec^{-2}	Applied acceleration = 470.88 m sec^{-2}
C1	5.5399 pF	3.8964 pF
C2	5.7606 pF	15.037 pF
X	-49.368 nm	-1.3487 μm
Vmod	2.2141 V_{PP}	111.0 V_{PP}
Vdemod	0.75671 V	54.535 V

Table 3: Variation in voltage reference for all process corners

Corners	Variation (mV)
SS	±0.41
FF	±0.32
FS	±1.77
SF	±0.31
TT	±0.36

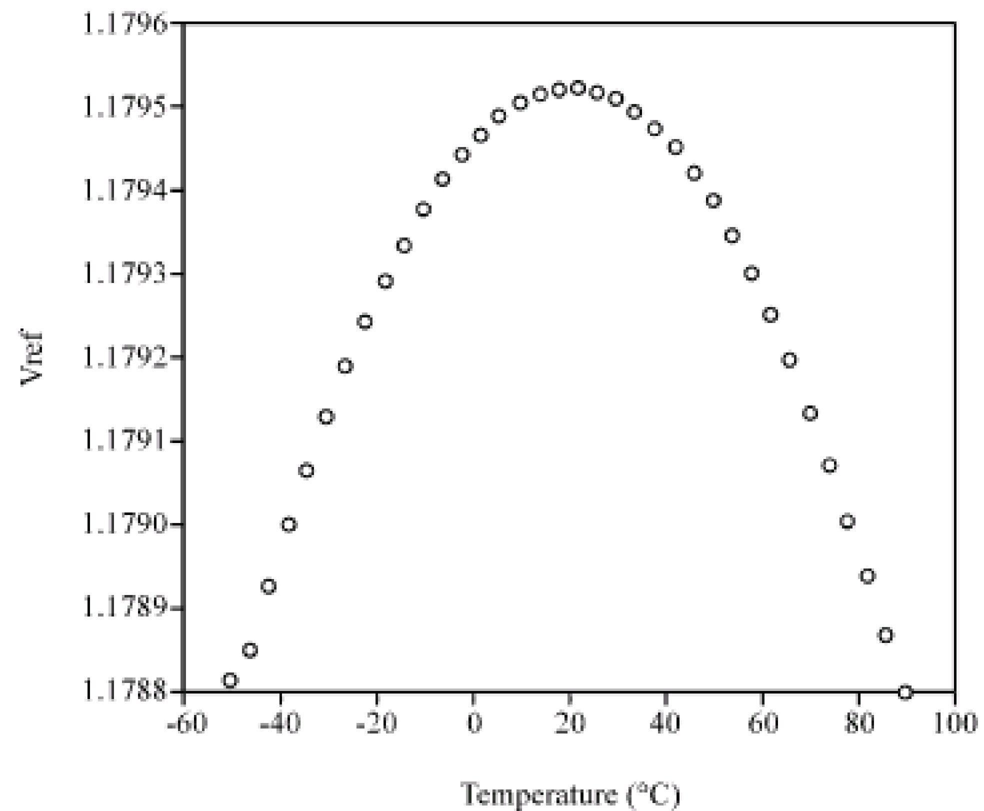

Fig. 17: Temperature variation of the output voltage of the BGR at typical condition

over temperature at typical condition and in all process corners is shown in Fig. 17 and 18, respectively. The summary of variation is shown in Table 3. The output reference exhibits ±0.614 mV variation from the mean value when the supply changes from 2.25 to 2.75 V (Fig. 19). The design achieves a maximum PSRR of -49.03 dB for frequency less than 18.5 kHz (Fig. 20). It is obvious that the proposed design achieves a small chip area, low peak-to-peak output variation for typical condition and high PSRR (Table 4).

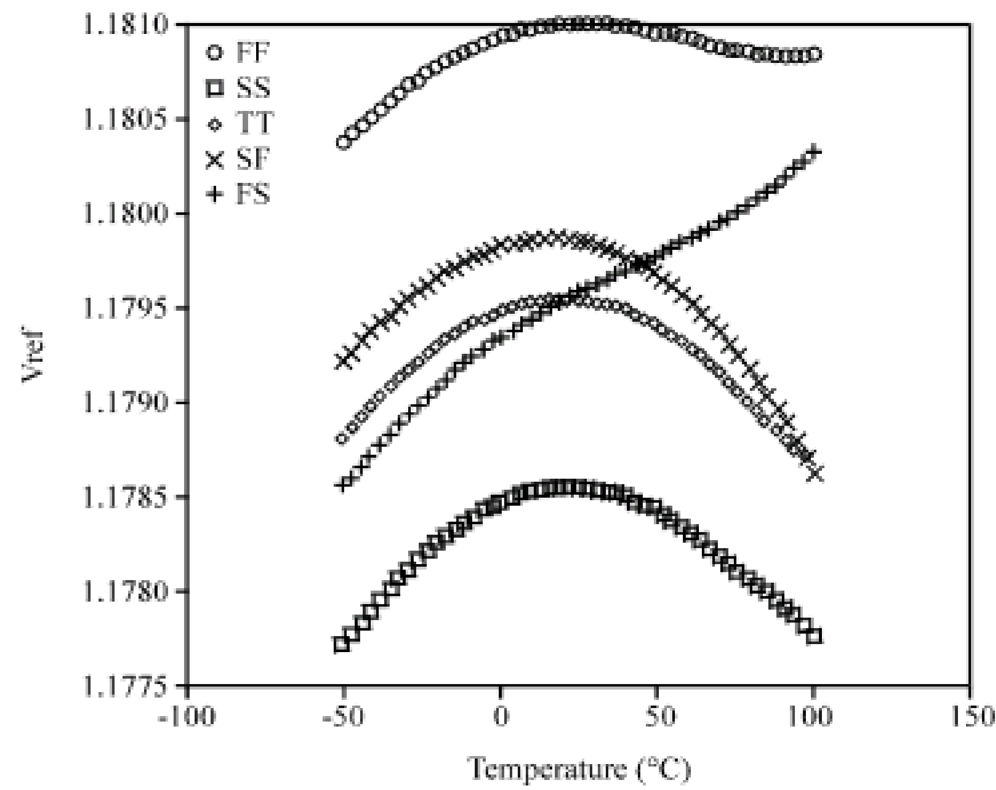

Fig. 18: Simulation result of the voltage reference vs. temperature in all process corner

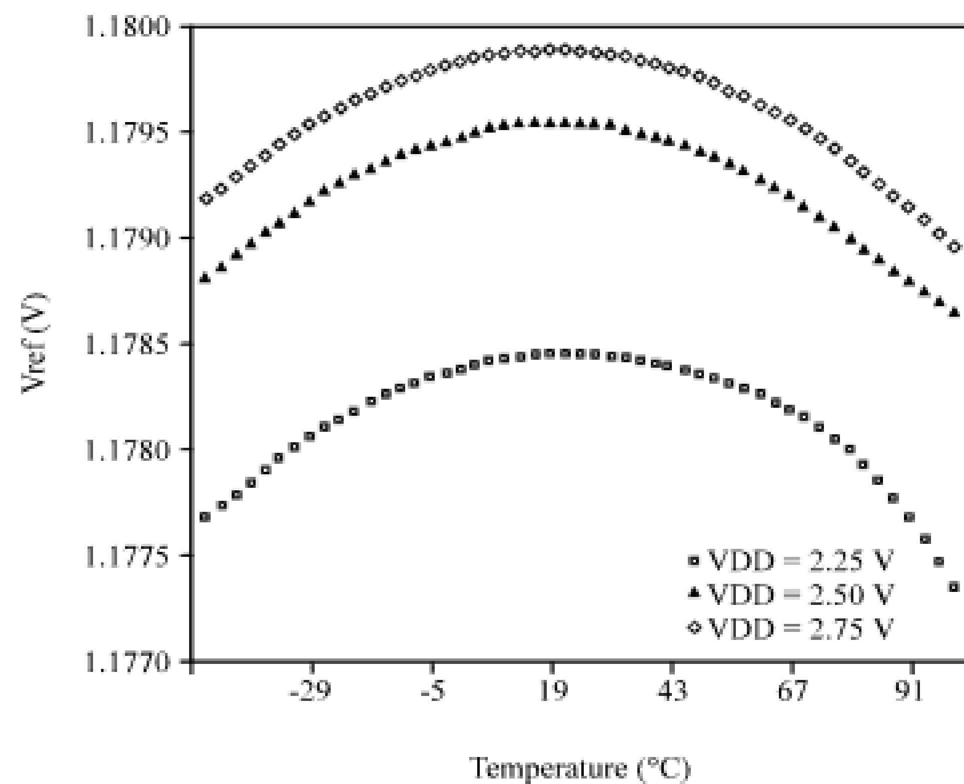

Fig. 19: Supply voltage variation of the output voltage of the BGR

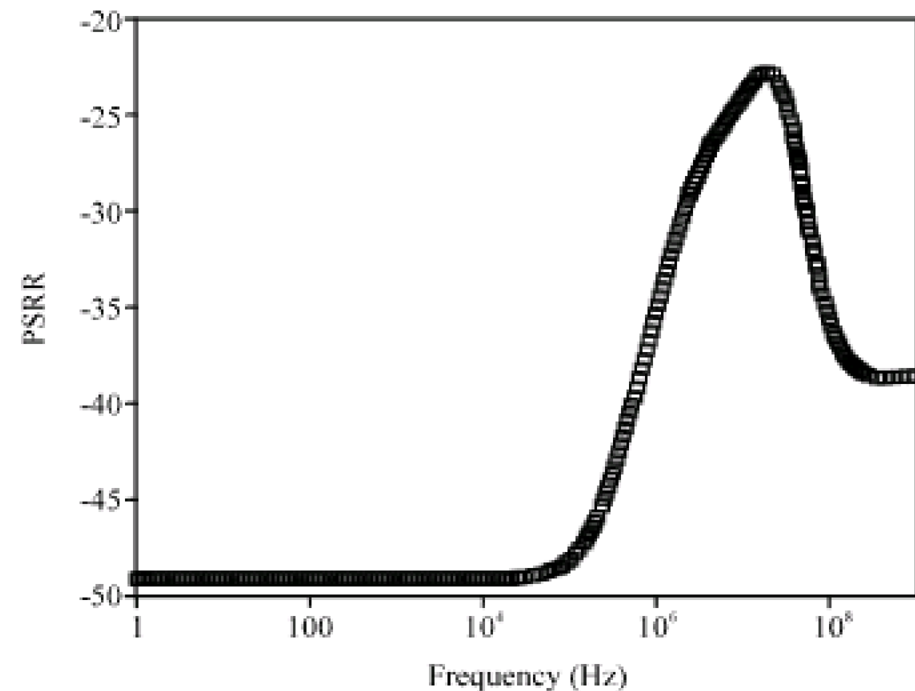

Fig. 20: Simulation result of PSRR of the proposed design at room temperature with 2.5 V supply

Table 4: Summary of the performance of the proposed BGR

Parameters	Post-layout
Chip area (core)	174.4×80.2 μm
Supply voltage	2.5
Reference voltage	1.17949 V
Peak-to-peak output variation (-50 to 100°C)	0.15 mV
PSRR @ 27°C	-49.03 @ 10 Hz
	-49.30 @ 1 kHz
	-35.19 @ 1 MHZ

CONCLUSION

Design, simulation and analysis of capacitive comb drive MEMS accelerometer using commercial software Coventorware® 2006 were presented in this current study. The structure uses proof mass suspended by four straight beams and interdigitated combs are used for driving the structure, as well as sensing capacitors to provide differential capacitance measurement. An analysis on the DC operating point, mechanical resonance frequency, vary, DC transfer and transient has been presented and discussed. A simplified analytical model to explain the analysis is also presented. The results obtained by simulation were in close agreement with the analytical results.

A very low voltage variation in BGR has also been presented. The proposed design produces an output voltage reference of 1.175837 over a temperature range from -50 to 150°C. The reference voltage has a variation of ±0.36 mV with temperature and exhibits ±0.614 mV variation from the mean value when the supply changes from 2.25 to 2.75 V. The design achieved a maximum PSRR of -49 dB for frequency less than 18.5 kHz.

ACKNOWLEDGMENTS

The authors would like to express sincere appreciation of the assistance of Mr. Mohd Kusairay Musa and Mr. Faisal Mohamad for his co-operation and assistance in providing support of the software. To Mr. Fazlan, Mr. Sanusi, Mr. Zamri and Puan Rohana, thanks for their kind help. Financial support from the Universiti Sains Malaysia Short Term Grant, 304/PELECT/6035301 is gratefully acknowledged.

NOMENCLATURE

η : No. of movable fingers
ε_0 : The permittivity of free space
ε_r : The relative permittivity of the dielectric
h : Thickness of the accelerometer
V : Voltage applied to the Straight Comb Bottom
y_0 : Initial capacitor length
y : Displacement in Y direction
x_+ : Initial lateral gap

x_{-} : Initial lateral gap
x : Displacement in X direction
k_{mech} : Mechanical spring constant
E : Young's modulus of silicon
h : Thickness of the accelerometer
w_b : Beam width
L_b : Beam length
W_m : Width of the rigid plate
L_m : Length of the rigid plate
W_f : Finger width
L_f : Finger length
η_x : No. of perforation holes in x direction
η_y : No. of perforation holes in y direction
H : Distance between the perforation holes in x and y directions
ρ : Density of silicon
m_S : Sensing mass
g : Acceleration due to gravity
k : Boltzmann's constant
q : Electron charge
T : Absolute temperature
n : Emitter area

REFERENCES

Bernhard, E.B. and R.T. Howe, 1996. Surface Micromachined Accelerometers. IEEE J. Solid State Circuits, 31: 366-375.

Chih-Ming, S., W. Chuanwei and F. Weileun, 2008. On the sensitivity improvement of CMOS capacitive accelerometer. Sensors Actuators A Physical, 141: 347-352.

Dan, H., 2000. A low-cost micromechanical accelerometer with integrated solid-state sensor. Sensors Actuators A Physical, 84: 149-155.

Fokhrul, I.M.D., M.A.M. Ali and Y.M. Burhanuddin, 2008. RF MEMS-based tunable filter for X-band applications. J. Applied Sci., 8: 189-191.

Gang, Z., X. Huikai, E.R. Lauren and K.F. Gary, 1999. A lateral capacitive CMOS accelerometer with structural curl compensation. Proceedings of the 12th IEEE International Conference on Micro Electro Mechanical Systems (MEMS), Jan. 17-21, Orlando, IEEE, pp: 606-611.

John, K.C., H.J.F. Colin, M.W. Stewart and R.M. Alan, 2008. Application of optimal and robust design methods to a MEMS accelerometer. Sensors Actuators A Physical, 142: 88-96.

Josselin, V., P. Touboul and R. Kielbasa, 1999. Capacitive detection scheme for space accelerometers applications. Sensors Actuators A Physical, 78: 92-98.

Junseok, C., K. Haluk and N. Khalil, 2005. A monolithic Three-Axis Micro-g Micromachined silicon capacitive accelerometer. J. Microelectromechanical Syst., 14: 235-242.

Ka Nang, L., P.K.T. Mok and L. Chi Yat, 2003. A 2-V 23 μA 5.3 ppm/°C curvature-compensated CMOS bandgap voltage reference. IEEE J. Solid State Circuits, 38: 561-564.

Krishnamoorthy, U., R.H. Olsson, G.R. Bogart, M.S. Baker, D.W. Carr, T.P. Swiler and P.J. Clews, 2008. In-plane MEMS-based nano-g accelerometer with sub-wavelength optical resonant sensor. Sensors Actuators A Physical, 145-146: 283-290.

Rasoul, D. and S.M. Atarodi, 2003. A new low voltage precision CMOS current reference with no external components. IEEE Trans. Circuits Syst. Analog Digital Signal Process., 50: 928-932.

Razavi, B., 2000. Design of Analog CMOS Integrated Circuits. 1st Edn., McGraw-Hill, USA, New York, ISBN: 9780072372717.

Rincon, M. and G. Alfonso, 2001. Voltage References: From Diodes to Precision High-Order Bandgap Circuits. 1st Edn., Wiley-IEEE Press, USA, ISBN: 978-0-471-14336-9.

Seiji, A., K. Sho, Y. Daiichiro and I. Yuichi, 2007. Surface micromachined accelerometer using ferroelectric substrate. Sensors Actuators A Physical, 139: 88-94.

Tan, C.W. and S. Park, 2002. Design and error analysis of accelerometer-based inertial navigation systems. California partners for advanced transit and highways (PATH). Research Reports: Paper UCB-ITS-PRR-2002-21. http://repositories.cdlib.org/cgi/viewcontent.cgi?article=1563andcontext=its/path.

Vivek, A., T.K. Bhattacharayya and S. Banik, 2006. Design steps for bulk micro machined single axis silicon capacitive accelerometer with optimized device dimensions. J. Physics Int. MEMS Conf., 34: 722-727.

Xingguo, X., W. Yu-Liang and J. Wen-Ben, 2005. Design and analysis of self-repairable MEMS accelerometer. Proceedings of the 20th International Symposium on Defect and Fault Tolerance in VLSI Systems (DFT 2005), Oct. 3-5, Monterey, IEEE, pp: 21-32.

Zimmermann, L., J.P. Ebersohl, F.L. Hung, J.P. Berry, F. Baillieu, P. Rey, B. Diem, S. Renard and P. Caillat, 1995. Airbag application: A microsystems including a silicon capacitive accelerometer, CMOS switched capacitor electronics and true self-test capability. Sensors Actuators A Physical, 46: 190-195.